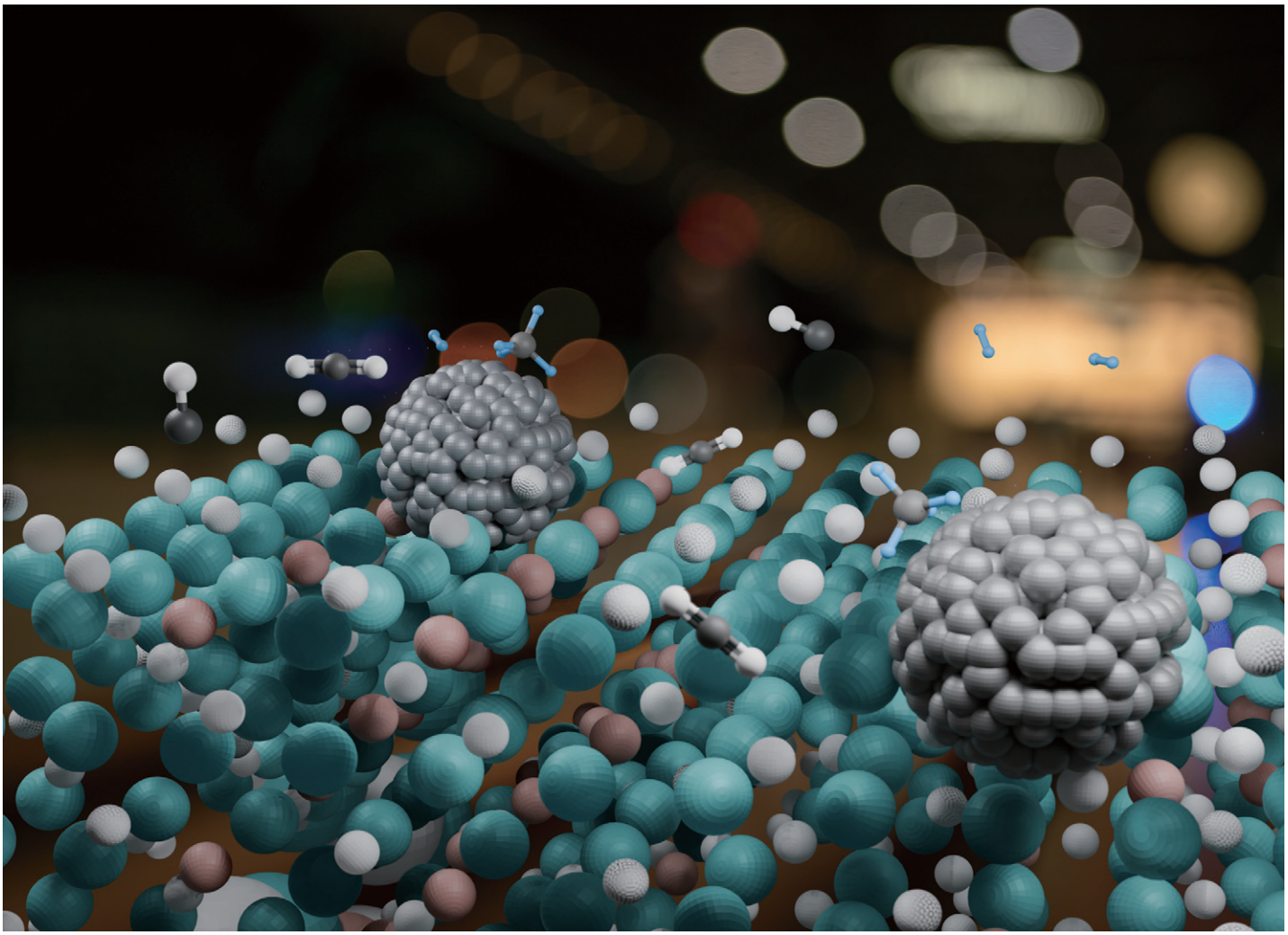

Showcasing research from Professor Zhou's laboratory, Department of Chemistry, University of Wyoming, Wyoming, US.

Effect of Ti dopants in $Ce_{1-x}Ti_xO_{2-\delta}$-supported Ni catalysts: structure, redox properties, and carbon resistance in DRM

5 wt.% Ni was prepared over $Ce_{1-x}Ti_xO_{2-\delta}$ ($0 \le x \le 0.5$, $0 < \delta < 0.5$) for dry reforming of methane (DRM). At low Ti compositions ($x < 0.3$), Ti can be well incorporated into the ceria lattice to form $Ce_{1-x}Ti_xO_{2-\delta}$ mixed oxides. Additional TiO_2 crystallites were formed over $Ce_{1-x}Ti_xO_{2-\delta}$ with higher Ti compositions. Combined spectroscopy and microscopy studies demonstrate that Ti dopant can modify crystal structures and redox properties of ceria, influence the metal-support interaction and the formation of Ni species (NiO and $NiTiO_3$), and thus affect their activity, stability, and carbon resistance in DRM.

Image reproduced by permission of Jintao Miao, Nishan Paudyal, Rosa V. Melinda & Jing Zhou from *Catal. Sci. Technol.*, 2025, **15**, 7030.

As featured in:

See Jing Zhou *et al.*, *Catal. Sci. Technol.*, 2025, **15**, 7030.

ROYAL SOCIETY OF CHEMISTRY

rsc.li/catalysis

Registered charity number: 207890

Catalysis Science & Technology

ROYAL SOCIETY OF CHEMISTRY

PAPER

View Article Online
View Journal | View Issue

Check for updates

Cite this: *Catal. Sci. Technol.*, 2025, **15**, 7030

Effect of Ti dopants in $Ce_{1-x}Ti_xO_{2-\delta}$-supported Ni catalysts: structure, redox properties, and carbon resistance in DRM

Jintao Miao, Nishan Paudyal, Rosa V. Melinda and Jing Zhou *

Received 22nd June 2025,
Accepted 27th August 2025

DOI: 10.1039/d5cy00760g

rsc.li/catalysis

In this study, 5 wt% Ni catalysts over a series of $Ce_{1-x}Ti_xO_{2-\delta}$ supports with controlled Ti dopant composition (x = 0–0.5) were synthesized by sol–gel and impregnation methods. Compositions, crystal structures, and surface properties were investigated to confirm the formation of $Ce_{1-x}Ti_xO_{2-\delta}$ mixed oxides with low Ti compositions (*e.g.*, $Ce_{0.9}Ti_{0.1}O_{2-\delta}$). Ce^{4+} in Ce–O–Ti shows a lower reduction temperature compared to bulk Ce^{4+} in $CeO_{2-\delta}$, and thus Ti-doped ceria exhibits better reducibility. TiO_2 is also formed over $Ce_{1-x}Ti_xO_{2-\delta}$ with high Ti compositions (*e.g.*, $Ce_{0.5}Ti_{0.5}O_{2-\delta}$), suggesting the limited solubility of Ti in the ceria lattice. The amount of Ti in $Ce_{1-x}Ti_xO_{2-\delta}$ plays a role in the formation of Ni species. NiO was found to be the major species over $CeO_{2-\delta}$ and $Ce_{0.9}Ti_{0.1}O_{2-\delta}$. However, $NiTiO_3$ was observed over $Ce_{1-x}Ti_xO_{2-\delta}$ ($x \geq 0.2$). Compared to Ni/$CeO_{2-\delta}$, Ni/$Ce_{0.9}Ti_{0.1}O_{2-\delta}$ delivers better CH_4 and CO_2 conversions in DRM. This can be attributed to the enhanced reducibility of $Ce_{0.9}Ti_{0.1}O_{2-\delta}$ and the stronger metal–support interaction by a small amount of Ti doping in ceria. The DRM activity of Ni decreases with the increased Ti composition in Ni/$Ce_{0.5}Ti_{0.5}O_{2-\delta}$. This can be correlated with the formation of $NiTiO_3$, which produces significantly less metallic Ni as the active species for DRM compared to NiO that is formed over $CeO_{2-\delta}$ and $Ce_{0.9}Ti_{0.1}O_{2-\delta}$. The TGA results of spent catalysts indicate a decrease in carbon deposition during DRM with increasing Ti composition in Ni/$Ce_{1-x}Ti_xO_{2-\delta}$. XRD data suggest the formation of a new $Ce_2Ti_2O_7$ phase in spent Ni/$Ce_{0.5}Ti_{0.5}O_{2-\delta}$, which could better help remove carbon deposits. Doping Ti into the ceria lattice significantly helps mitigate the issue related to carbon deposition over the Ni catalyst during DRM. Similar behavior was also observed over $Ce_{1-x}Ti_xO_{2-\delta}$-supported Co catalysts. Our study clearly demonstrates that doping Ti in ceria can tune both the activity and stability of supported metal catalysts in DRM.

Introduction

Dry reforming of methane (DRM, $CH_4 + CO_2 \rightarrow 2H_2 + 2CO$, ΔH_{298K} = +247 kJ mol^{-1}) has attracted attention over recent decades because of (a) simultaneous utilization of two major greenhouse gases (CH_4 and CO_2) and (b) the ability to produce syngas (mixture of H_2 and CO) over heterogeneous catalysts.[1–5] The reaction involves activation of C–H and C–O bonds followed by a subsequent reaction to produce CO and H_2.[6] Oxide-supported metal catalysts, particularly Ni/CeO_2, have been widely studied as potential catalysts.[7,8] The overall activity depends on the type of the active metal, the nature of the support, and the interaction between the metal and support. It is commonly accepted that the reaction mechanism is bifunctional.[9] Methane and CO_2 can be activated on the metal and support, respectively. The interface between the metal and the metal oxide provides sites to complete the reaction. Ni is an active metal for breaking the C–H bond.[10–12] Furthermore, it is more cost-effective as practical catalysts compared to noble metals.[13] However, Ni is more prone to deactivation, especially due to carbon deposition.[14] Side reactions in DRM including methane decomposition and the Boudouard reaction can result in carbon deposition over Ni catalysts, blocking the active sites for further reaction.[15,16] Ceria has been studied as a viable support to Ni. Due to its unique redox properties and oxygen storage capacity, ceria could act as the active phase to help remove C deposits on the Ni metal by oxidation of surface carbon as CO.[17,18] It has been shown that the Ni/CeO_2 catalyst exhibits a promising catalytic behavior as a result of the unique metal–support interaction.[11,19–21]

Doping of ceria with other metal cations can enhance the thermal stability as well as the redox properties of ceria and thus better improve the activity and stability of Ni in DRM.[22,23] Various metal elements have been selected as dopants to prepare doped ceria, including Zr, La, Ti, and Mg.[24–28] Ti was found to be a good candidate as a dopant based on both computational and experimental work.[29,30] Compared to pure ceria, Ti-doped ceria has a lower formation energy of oxygen

Department of Chemistry, University of Wyoming, Laramie, WY 82071, USA. E-mail: jzhou2@uwyo.edu

vacancies, which enhances the oxygen mobility in the ceria lattice.[31,32] The Ce/Ti ratio was found to be an important parameter in tuning the redox properties of ceria. Efstathiou's group prepared $Ce_{0.8}Ti_{0.2}O_{2-\delta}$ and $Ce_{0.5}Ti_{0.5}O_{2-\delta}$ supports for Ni and Pt catalysts and examined their catalytic performance for DRM and water–gas shift (WGS) reactions.[33–35] They reported a better carbon resistance behavior over $Ni/Ce_{0.8}Ti_{0.2}O_{2-\delta}$ than over $Ni/CeO_{2-\delta}$ and $Ni/Ce_{0.5}Ti_{0.5}O_{2-\delta}$, which is attributed to the effect of the particle size and supports. Since the effect of the particle size and support are usually coupled, in an attempt to decouple these two factors, Han and co-workers prepared Ni-based catalysts over various supports with controlled particle sizes. They suggested that a small particle size of Ni particles and their interaction with a basic metal oxide support are beneficial to the performance in DRM.[36] In our previous study, we prepared well-ordered $CeO_2(111)$ thin films as well as $Ce_{1-x}Ti_xO_{2-\delta}(111)$ thin films over Ru(0001) under ultra-high vacuum (UHV) conditions. We found that Ti-doped ceria can better anchor Ni as smaller particles and help inhibit its sintering with heating to 800 K than pure ceria.[31] Sintering of Ni at high reaction temperatures also causes catalyst deactivation.[16,36] Smaller metal particles not only provide more active sites for the reaction, but also minimize carbon formation.[36,37] To extend the exciting observation from the model system of $Ni/Ce_{1-x}Ti_xO_{2-\delta}(111)$ thin films, we synthesized powder materials of $Ce_{1-x}Ti_xO_{2-\delta}$ with controlled Ti compositions by sol–gel methods and dispersed 5 wt% Ni over as-synthesized supports by impregnation methods. The composition of Ti was controlled between $x = 0$ and $x = 0.5$. Compared to previous studies, a smaller increment of the Ti composition (*i.e.*, 0.1) was considered with a motivation to better tune the structure and redox properties of ceria and thus examine potential improvement of supported Ni catalysts towards the DRM reaction and carbon resistance.[33,35] In our study, conventional and synchrotron X-ray diffraction (XRD), X-ray photoelectron spectroscopy (XPS), scanning electron microscopy (SEM), inductively coupled plasma-optical emission spectrometry (ICP-OES), Brunauer–Emmett–Teller (BET), H_2-temperature-programmed reduction (H_2-TPR), and H_2 chemisorption were used to examine the composition, the crystal structure, the reducibility, and the surface properties of prepared Ni catalysts with respect to the Ti composition in ceria. XRD and thermogravimetric analysis (TGA) were used to examine the structure and the extent of carbon deposition over spent catalysts. This systematic study using combined spectroscopy and microscopy techniques allowed for the elucidation of the role of Ti doping in ceria in the activity, stability, and carbon resistance of supported Ni in DRM. It was found that, by doping Ti into the ceria lattice, significant enhancement in the reducibility of the supports as well as the metal–support interaction was observed. Furthermore, the amount of Ti dopant plays a role in the nature of Ni species including NiO and $NiTiO_3$ formed over $Ce_{1-x}Ti_xO_{2-\delta}$, which exhibits a strong correlation with their physical properties and catalytic performance in DRM. Such behavior was also observed for Co catalysts over Ti-doped ceria.

Experimental section

Catalyst preparation

$Ce_{1-x}Ti_xO_{2-\delta}$ with controlled Ti composition ($0 \le x \le 0.5$) was prepared by mixing appropriate amounts of cerium(III) nitrate hexahydrate (Sigma Aldrich, 99.99%) and titanium(IV) isopropoxide (Sigma Aldrich, ≥ 97%) with citric acid (Fisher Scientific, 99.6%), following a reported synthesis procedure with a modified calcination temperature of 800 °C.[34] For example, 7.0785 g of citric acid, 9.5937 g of cerium(III) nitrate hexahydrate, and 13.0 mL of titanium(IV) isopropoxide stock solution (0.200 mol L^{-1}) were used for the preparation of $Ce_{0.9}Ti_{0.1}O_{2-\delta}$. The mixture was heated at 60 °C under constant stirring at a speed of 500 rounds per minute until a gel-like material was obtained. The material was then dried in an oven at 120 °C overnight and subsequently calcined in a tube furnace (GSL-1500X, MTI corporation) at 800 °C for 2 h in ambient air. Supported Ni catalysts with a nominal loading of 5 wt% were prepared by the impregnation method by weighing out appropriate amounts of selected $Ce_{1-x}Ti_xO_{2-\delta}$ support of interest and nickel(II) nitrate hexahydrate (Sigma Aldrich, 99.999%). The mixture was stirred for 2 h at 60 °C followed by drying overnight at 120 °C. The dried powder was further calcined at 800 °C for 2 h in the tube furnace and stored into an airtight container for further tests. In our study, the choice of Ni amount was based on our DRM results with respect to controlled weight loadings of Ni over pure ceria supports (data not shown). We observed an increase in DRM activity with the increase of the Ni amount from 2 to 5 wt%. Further increase of the Ni loading to 7 wt% did not introduce any detectable change in the DRM activity, while exhibiting a larger extent of carbon formation. The choice of 5 wt% Ni over $Ce_{1-x}Ti_xO_{2-\delta}$ for DRM in our study is also consistent with previous research over 4 wt% Ni over $CeZrO_2$ considering that the interaction between Ni and ceria plays an important role in DRM.[27] δ was introduced in the stoichiometry of $Ce_{1-x}Ti_xO_{2-\delta}$ to suggest that the supports are partially reduced as indicated by XPS studies shown in Fig. S1 in the SI. Like Ni catalysts, ceria-supported Co catalysts can be prepared following the steps using cobalt(II) nitrate hexahydrate (Sigma Aldrich, >98%).

Catalyst characterization

Conventional XRD experiments of the as-prepared and spent catalysts were performed on a Rigaku SmartLab diffractometer with Cu Kα radiation (40 kV, 40 mA, 1.5419 Å) in a 2-theta mode from 10 to 90° at a scanning rate of 10° min^{-1} with a step size of 0.01°. *In situ* synchrotron XRD was conducted at the beamline (BM-17) at the Advanced Photon Source, Argonne National Laboratory. Around 1 mg sample was loaded in a capillary quartz tube with quartz wool at both ends to contain the sample. The XRD data were collected upon heating the sample from 20 to 750 °C with a ramping rate of 30 °C min^{-1} under a mixture gas flow of 5 mL min^{-1} H_2 and 5 mL min^{-1} He. The synchrotron XRD data were first processed using the GSAS-II software.[38] All XRD patterns were

analyzed for peak positions to examine the structure and crystallinity of the samples using the ICDD database. The lattice constant and crystallite size of CeO_2 were calculated based on Bragg's law and the Scherrer equation. The BET surface area of the samples was obtained by N_2 physisorption using a Micromeritics ASAP 2020 apparatus. Prior to the analysis, all powder samples were degassed at 300 °C for 3 h under vacuum conditions. H_2-TPR and H_2 chemisorption experiments were conducted using a Micromeritics AutoChem II 2920 instrument equipped with a thermal conductivity detector. For H_2-TPR experiments, around 0.05 g of the sample was heated from room temperature to 850 °C with a ramp rate of 10 °C min^{-1} under 25 mL min^{-1} 10% H_2 in Ar flow (Praxair) and held for 5 min at 850 °C. The metal dispersion was collected over 0.3 g of the sample at 35 °C using H_2 pulse measurement. Prior to the test, the sample was reduced at 750 °C for 1 h, followed by purging with 50 mL min^{-1} Ar at 750 °C. It was noted that the reduction temperature of all samples from *in situ* synchrotron XRD experiments was consistently lower than that from H_2-TPR tests, which could be due to the higher H_2 concentration and gas hourly space velocity (GHSV) for the XRD experimental setup.[39,40] The XPS experiments of the as-prepared and reduced Ni/$Ce_{1-x}Ti_xO_{2-\delta}$ samples were conducted with a HiPP Omicron Nanotechnology XPS system. For the experiment of reduced samples, catalysts were reduced at 750 °C for 1 h under 50 mL min^{-1} H_2 flow and then kept in airtight vials. ICP-OES experiments were conducted using a PerkinElmer Optima 8300 instrument. The SEM studies were carried out using an FEI Quanta FEG 450 instrument with an accelerating voltage of 20 kV. For the preparation, the sample was dissolved using the fusion method. $LiBO_2$ (Sigma-Aldrich, 99.99%) was chosen as the flux and the solid mixture of the flux and sample was calcined at 900 °C in a graphite crucible. The TGA tests were conducted using Netzsch TG 209 instruments. The sample was first purged with 50 mL min^{-1} O_2 at room temperature and then ramped up to 750 °C with a heating rate of 5 °C min^{-1}.

Catalyst reaction

The DRM reactions were performed in a fixed-bed reactor with controlled temperatures and feed flow rates. Around 0.1 g of the sample was loaded in a quartz tube (1/4 inch inner diameter) with quartz wool on both ends. The sample was heated in a vertical tube furnace (Keison Products, VST 1200). The flow rates of all gases were controlled using digital mass flow controllers (Aalborg). The reaction gas composition was analyzed using an Agilent 7890B instrument equipped with both a thermal conductivity detector and a flame ionization detector. The conversions of CH_4 and CO_2 as well as the yields of H_2 and CO were calculated *via* the following equations:

$$CH_4\ \text{Conversion}\ (\%) = \frac{\text{input}\ [F_{CH_4}] - \text{output}\ [F_{CH_4}]}{\text{input}\ [F_{CH_4}]} \times 100\% \quad (1)$$

$$CO_2\ \text{Conversion}\ (\%) = \frac{\text{input}\ [F_{CO_2}] - \text{output}\ [F_{CO_2}]}{\text{input}\ [F_{CO_2}]} \times 100\% \quad (2)$$

$$H_2\ \text{Yield}\ (\%) = \frac{\text{output}\ [F_{H_2}]}{2 \times \text{input}\ [F_{CH_4}]} \times 100\% \quad (3)$$

$$CO\ \text{Yield}\ (\%) = \frac{\text{output}\ [F_{CO}]}{\text{input}\ [F_{CH_4}] + \text{input}\ [F_{CO_2}]} \times 100\% \quad (4)$$

where $[F_i]$ indicates the flow rate (in mL min^{-1}) of gas species i (i = CH_4, CO_2, H_2, and CO).

Results and discussion

To examine the effect of Ti doping on the properties of ceria and ceria-supported Ni catalysts, a series of $Ce_{1-x}Ti_xO_{2-\delta}$ supports with controlled amounts of Ti up to x = 0.5 were prepared. The elemental composition of Ti was examined by ICP-OES and the measured values (Table 1) agree well with the nominal numbers as intended during the synthesis. As suggested by the XRD pattern (Fig. 1a), the synthesized $CeO_{2-\delta}$ sample exhibits high crystallinity. Sharp reflection peaks at around 28.5°, 33.1°, 47.5°, 56.3°, 59.1°, 69.4°, 76.7°, 79.1°, and 88.4° match well with the (111), (200), (220), (311), (222), (400), (331), (420), and (422) planes of the face-centered cubic cell of the fluorite structure of CeO_2 (PDF #34-0394). With addition of Ti into CeO_2, a line broadening and an upward shift in the peak positions were observed. As shown in Table 1, with an initial 10% Ti doping amount, the crystallite size of ceria significantly decreases from 298 to 142 Å and further increase of the doping amount of Ti causes less change in the crystallite size. This decreasing trend of the crystallite size with the increase of Ti concentration is consistent with previously reported results.[30,41] The lattice constant of ceria calculated based on the analysis of the (111) plane showed a change from 5.41 to 5.39 Å with Ti doping concentration up to 0.5. This is consistent with the substitution of Ce^{4+} with Ti^{4+} into the ceria lattice that has a smaller radius.[42,43] Due to the difference in the metal–oxygen bonds, incorporation of Ti into the ceria lattice can result in the distortion in the crystal structure and the formation of the charge compensation oxygen vacancies.[44,45] Therefore, in our study, it is reasonable to expect and as shown in Fig. S1 in the SI that $Ce_{1-x}Ti_xO_{2-\delta}$ supports are partially reduced. The structure distortion and formation of vacancies can promote the oxygen storage capacity and redox properties of ceria that are important for catalytic reactions.[23,46–48] For ceria supports with relatively high Ti compositions, a new reflection peak at 25.3° was shown, which is associated with TiO_2 (PDF #29-1360), suggesting the limited solubility of Ti in the ceria lattice. This reflection peak was broad for $Ce_{0.7}Ti_{0.3}O_{2-\delta}$, but it became sharper and more intense with further increase of the Ti stoichiometry for $Ce_{0.6}Ti_{0.4}O_{2-\delta}$ and $Ce_{0.5}Ti_{0.5}O_{2-\delta}$ samples. Ti can be well incorporated into the ceria lattice with low Ti compositions ($x < 0.3$) to form $Ce_{1-x}Ti_xO_{2-\delta}$

Table 1 Indicated physical properties of pure $CeO_{2-\delta}$ and $Ce_{1-x}Ti_xO_{2-\delta}$

$Ce_{1-x}Ti_xO_{2-\delta}$	Ti composition, x, by ICP-OES	Lattice constant (Å)	Crystallite size (Å)	BET surface area ($m^2\ g^{-1}$)	Metal dispersion of supported Ni catalysts (%)
$CeO_{2-\delta}$	0	5.413	298	13.7	1.2
$Ce_{0.9}Ti_{0.1}O_{2-\delta}$	0.10	5.403	142	15.2	1.0
$Ce_{0.8}Ti_{0.2}O_{2-\delta}$	0.22	5.403	127	17.0	0.3
$Ce_{0.7}Ti_{0.3}O_{2-\delta}$	0.32	5.394	125	12.6	0.3
$Ce_{0.6}Ti_{0.4}O_{2-\delta}$	0.42	5.392	119	8.8	0.4
$Ce_{0.5}Ti_{0.5}O_{2-\delta}$	0.51	5.394	121	8.8	0.3

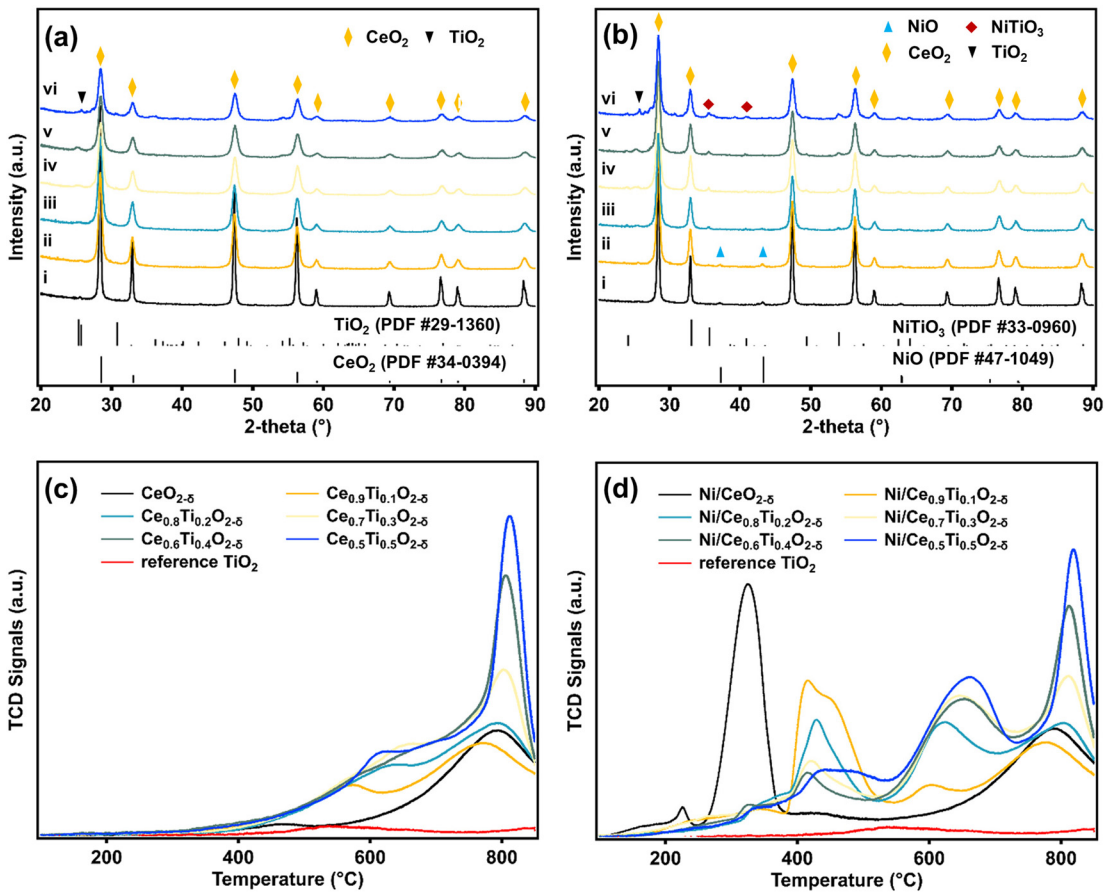

Fig. 1 XRD patterns of (a) $Ce_{1-x}Ti_xO_{2-\delta}$ supports and (b) 5 wt% Ni over $Ce_{1-x}Ti_xO_{2-\delta}$ with controlled Ti compositions (i: x = 0, ii: x = 0.1, iii: x = 0.2, iv: x = 0.3, v: x = 0.4, vi: x = 0.5). Reference XRD patterns of TiO_2, CeO_2, $NiTiO_3$, and NiO are also shown. H_2-TPR profiles collected from (c) as-prepared $Ce_{1-x}Ti_xO_{2-\delta}$ and (d) 5 wt% Ni dispersed over $Ce_{1-x}Ti_xO_{2-\delta}$. H_2-TPR profiles of a reference TiO_2 sample are also shown in (c) and (d).

mixed oxides. However, when further introducing Ti with heating during the synthesis, additional TiO_2 crystallites were formed. This is consistent with reported studies of $Ce_{1-x}Ti_xO_2$.[34,49,50] Segregation from the ceria lattice and formation of titania are dependent on synthesis methods and temperatures, which was reported for $Ce_{1-x}Ti_xO_2$ with a Ti composition, x, of as low as 0.2.[26,51] Mordekovitz and co-workers synthesized $Ce_{1-x}Ti_xO_2$ nanomaterials (x = 0.1, 0.2) using a non-aqueous sol–gel method. There was no indication of isolated domains of titania in the XRD patterns of these products that were calcined at 400 °C. $Ce_{0.9}Ti_{0.1}O_2$ and $Ce_{0.8}Ti_{0.2}O_2$ samples were stable with heating to 700 °C. However, starting with the heating temperature of 800 °C, the TiO_2 phase was clearly observed in the XRD pattern of $Ce_{0.8}Ti_{0.2}O_2$.[51] Isolated domains of TiO_2 were also observed for the $Ce_{0.8}Ti_{0.2}O_2$ sample by Kim and co-workers, where the sample was calcined to a temperature of 850 °C.[26]

The reducibility of the same series of $Ce_{1-x}Ti_xO_{2-\delta}$ supports was examined by performing H_2-TPR experiments in a temperature range between 50 and 850 °C (Fig. 1c). The H_2-TPR profile of a standard TiO_2 powder sample (Sigma-Aldrich, ≥99.5%) is also shown, which exhibits little signal in this temperature range. To deconvolute the reduction features originating from different species formed over each sample, the

peak fitting of the H_2-TPR results was conducted using Voigt functions in the Fityk software and the detailed fitting information can be found in Fig. S2a and Table S1 in the SI. Reduction in two temperature ranges with peaks at ~481 and 791 °C was observed for $CeO_{2-\delta}$, which can be attributed to the reduction of surface and bulk Ce^{4+}, respectively.[34,52,53] The surface area and crystallite size of CeO_2 significantly affect the peak intensity and reduction temperature of both surface and bulk Ce^{4+}. Rao reported the synthesis of CeO_2 samples with the surface area values ranging from 1.5 to 130 $m^2\ g^{-1}$ and the characterization of the reducibility using H_2-TPR.[53] For the sample with a surface area value of 1.5 $m^2\ g^{-1}$, ignorable reduction of surface Ce^{4+} species was detected and only reduction of bulk Ce^{4+} was observed at 900 °C. When the surface area value was increased to 130 $m^2\ g^{-1}$, surface reduction features between 200 and 600 °C were clearly observed and the bulk reduction temperature decreased to 800 °C. In our study, for the ceria support with a 10% Ti dopant amount, the reduction temperature of bulk Ce^{4+} in ceria decreases to ~763 °C. This is consistent with the decrease in its crystallite size and surface area as well as the formation of reduced ceria as a result of Ti doping that exhibits enhanced reducibility.[34] Additional reduction signals between 400 and 650 °C over $Ce_{1-x}Ti_xO_{2-\delta}$ can be associated with Ce^{4+} in Ce–O–Ti that has a lower reduction temperature compared to bulk Ce^{4+} in $CeO_{2-\delta}$.[54,55] Doping additional metal cations (*e.g.*, Zr, Nb, and Ti) into the ceria lattice can modify the metal–oxygen bond length, which results in the formation of labile oxygen near Ce cations.[34,56,57] Thus, doped ceria usually exhibits a lower reduction temperature and higher oxygen storage capacity compared to pure ceria.[58] The intensity associated with the reduction of Ce^{4+} in Ce–O–Ti increases when the Ti composition (x) increases to 0.3. However, it shows no significant change with further increase in Ti composition to 0.5. A sharp reduction peak at around 800 °C was observed in $Ce_{1-x}Ti_xO_{2-\delta}$ ($x \geq 0.3$) supports and the intensity of this peak increases while further increasing Ti composition. This peak could suggest a change in the bulk structure of ceria. Smal and co-workers observed a decrease in the reduction temperature of ceria supports modified with Ti dopant and detected a sharp reduction peak at around 792 °C with high Ti concentrations in ceria. They ran H_2-TPR on 5 wt% Ni over $Ce_{0.55}Ti_{0.45}O_2$ and $Ce_{0.65}Ti_{0.35}O_2$ and examined their crystal structures during the H_2-TPR experiment as well as after cooling down to room temperature. The pyrochlore structure of $Ce_2Ti_2O_7$ was detected after cooling down to room temperature.[59] In our study, after reduction, $Ce_2Ti_2O_7$ was also observed in $Ni/Ce_{0.5}Ti_{0.5}O_{2-\delta}$, while the fluorite structure of ceria was maintained for both $Ni/CeO_{2-\delta}$ and $Ni/Ce_{0.9}Ti_{0.1}O_{2-\delta}$ as shown in Fig. S3. It is known that ceria with a pyrochlore structure can have high oxygen mobility due to its disordered structure, which could assist in oxidizing deposited carbon during the DRM reaction.[60]

Pure ceria ($CeO_{2-\delta}$) and Ti-doped ceria with a low Ti composition of $x = 0.1$ and a high value of $x = 0.5$ ($Ce_{0.9}Ti_{0.1}O_{2-\delta}$ and $Ce_{0.5}Ti_{0.5}O_{2-\delta}$) were selected as representative samples to further examine the effect of Ti doping using *in situ* synchrotron XRD. The XRD data (Fig. 2a–c) were collected with 2-theta values between 0.500° and 16.500° while the sample was heated from 50 °C up to 750 °C with a rate of 30 °C min^{-1} under a mixture gas flow of 5 mL min^{-1} H_2 and 5 mL min^{-1} He. For comparison, the XRD data of $CeO_{2-\delta}$ with heating under an inert environment of a 10 mL min^{-1} He flow were also collected. All three samples exhibit XRD patterns consistent with the fluorite structure of CeO_2 (PDF #34-0394). In agreement with the results from conventional XRD experiments in Fig. 1a, the calculated lattice constant (Fig. 2d) decreases from 5.410 Å for $CeO_{2-\delta}$ to 5.394 Å for $Ce_{0.5}Ti_{0.5}O_{2-\delta}$ due to the substitution of Ti into the ceria lattice. With heating, the $CeO_{2-\delta}$ support under an inert He flow shows a gradual increase in the lattice constant from 5.410 Å at room temperature to 5.457 Å at 800 °C, consistent with the thermal expansion of ceria.[61–64] When switching the gas from He to H_2He, an increase in the lattice constant of $CeO_{2-\delta}$ with temperature due to thermal expansion was observed. Additionally, a more significant increase in the lattice constant was detected at around 675 °C. This is attributed to the reduction of Ce^{4+} to Ce^{3+} under a reducing environment as Ce^{3+} cations have a larger radius (1.14 Å) than Ce^{4+} (0.97 Å).[27,42,65] Such behavior was also observed for $Ce_{0.9}Ti_{0.1}O_{2-\delta}$ and $Ce_{0.5}Ti_{0.5}O_{2-\delta}$ during heating under a H_2He flow. However, the extensive change in the lattice constant associated with the Ce^{4+} reduction occurred at lower temperatures. This behavior agrees well with the above H_2-TPR results as well as the XPS data shown in Fig. S1 in the SI, suggesting the enhanced reducibility of ceria with Ti doping.

The XRD patterns of 5 wt% Ni dispersed over the series of $Ce_{1-x}Ti_xO_{2-\delta}$ supports (x = 0–0.5) were collected as shown in Fig. 1b. In addition to the reflections associated with ceria and titania, the peaks related to different Ni species were observed, demonstrating that the nature of the ceria supports plays a role in the formation of these Ni species. For $Ni/CeO_{2-\delta}$ and $Ni/Ce_{0.9}Ti_{0.1}O_{2-\delta}$, the peaks at 37.2° and 43.3° were detected, corresponding to the (111) and (200) planes of NiO (PDF #47-1049). The peaks at 35.7°, 40.9°, and 54.0° that are associated with the (110), (113), and (116) planes of $NiTiO_3$ (PDF #33-0960) were observed over $Ni/Ce_{0.8}Ti_{0.2}O_{2-\delta}$ and became more pronounced with further increase of Ti composition to 0.5 in $Ce_{1-x}Ti_xO_{2-\delta}$. The formation of $NiTiO_3$ is suggested due to the reaction of Ni with isolated domains of TiO_2 during the metal dispersion and calcination process with a temperature typically higher than 550 °C.[26,49,50,66–69]

The H_2-TPR profile of 5 wt% $Ni/CeO_{2-\delta}$ (Fig. 1d) shows reduction peaks at 213 and 312 °C, which are attributed to the reduction of surface and bulk NiO, respectively.[70,71] The detailed peak fitting results of H_2-TPR can be found in Fig. S2b and Table S2. For $Ni/Ce_{0.9}Ti_{0.1}O_{2-\delta}$, reduction peaks of NiO shift to 330 and 453 °C, suggesting that Ti doping can enhance the metal–support interaction. For $Ni/Ce_{1-x}Ti_xO_{2-\delta}$ with higher Ti compositions (x = 0.3–0.5), the major reduction peak was observed at around 650 °C. This temperature is higher than that for reduction of NiO over

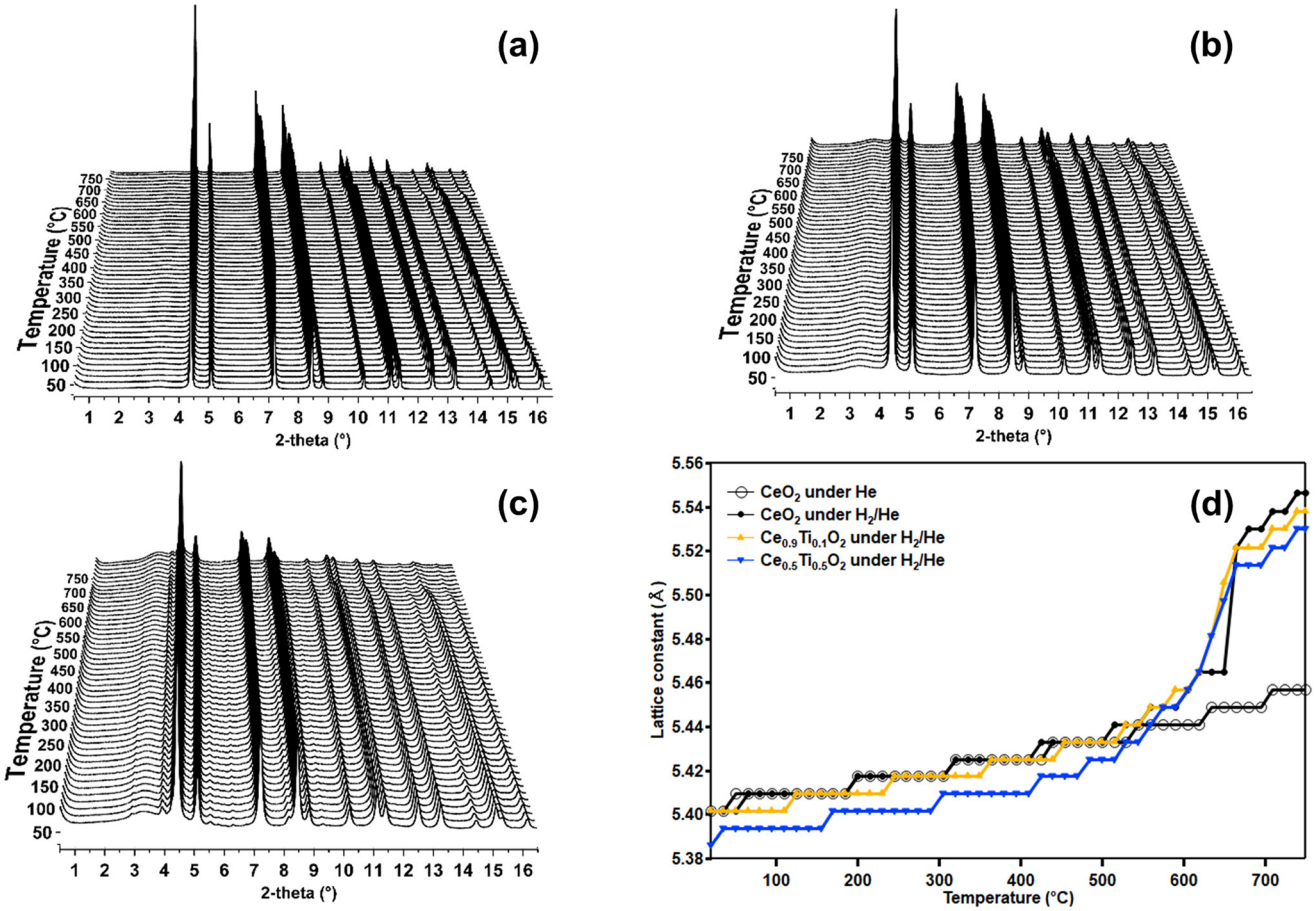

Fig. 2 (a)–(c): *In situ* synchrotron XRD patterns of $CeO_{2-\delta}$, $Ce_{0.9}Ti_{0.1}O_{2-\delta}$, and $Ce_{0.5}Ti_{0.5}O_{2-\delta}$ collected with heating from 50 to 750 °C under a flow of 5 mL min^{-1} H_2 and 5 mL min^{-1} He; (d) the calculated lattice constant of these three samples based on the (111) plane of CeO_2 with respect to temperature under the indicated gas species.

pure titania and is consistent with reduction of Ni^{2+} in $NiTiO_3$ that takes place in a temperature range between 550 and 700 °C.[49,50,68,69,72] The H_2-TPR data are consistent with the XRD results, demonstrating that doping $Ce_xTi_{1-x}O_{2-\delta}$ by Ti influences the formation of Ni species (*e.g.*, NiO and $NiTiO_3$). It seems like the nature of Ni species formed over the ceria support also affects the measured metal dispersion value of Ni as shown in Table 1. Despite the fact that the surface area values are not particularly high for $CeO_{2-\delta}$ and $Ce_{0.9}Ti_{0.1}O_{2-\delta}$, the metal dispersions of Ni over these two supports in our study are comparable with previously reported data.[73,74] However, the metal dispersion values of Ni decreased extensively with further increase in Ti composition to 0.3 or higher in $Ce_xTi_{1-x}O_{2-\delta}$. This is consistent with the observation that NiO is the major species over $CeO_{2-\delta}$ and $Ce_{0.9}Ti_{0.1}O_{2-\delta}$, while $NiTiO_3$ is formed over ceria supports with higher Ti compositions. During reduction, $NiTiO_3$ is reduced to metallic Ni and TiO_2, where Ni could be encapsulated by TiO_2 that could inhibit the adsorption of active gases (*e.g.*, H_2 and CO) over Ni and thus result in a low metal dispersion measured by chemisorption.[72,75] In addition to the formation of NiO over ceria, incorporation of Ni into its lattice to form a $Ce_{1-x}Ni_xO_{2-\delta}$ solid solution was reported, the extent of which depends on synthesis methods.[76–80] The XRD pattern of 5 wt% $Ni/CeO_{2-\delta}$ clearly shows the diffraction peaks associated with the NiO phase (Fig. 1b), which is consistent with the intense reduction peak at 312 °C in the H_2-TPR profile (Fig. 1d). In our study, there could be the possibility of incorporation of a small amount of Ni into the ceria lattice. A slight decrease in the lattice constant value of ceria from 5.413 Å for $CeO_{2-\delta}$ to 5.409 Å for $CeO_{2-\delta}$ with dispersed 5 wt% Ni was detected. Although this change in the lattice constant is within the range of the XRD resolution of the instrument, incorporation of Ni into the ceria lattice can cause the decrease of the lattice constant considering that Ni^{2+} has a smaller size (0.72 Å) than Ce^{4+} (0.97 Å).[80] When comparing the H_2-TPR profile of 5 wt% $Ni/CeO_{2-\delta}$ to that of pure $CeO_{2-\delta}$ (Fig. 1c and d), it shows small, enhanced signals between 350 and 650 °C. This could be due to the reduction of NiO that strongly interacts with ceria and/or the reduction of the ceria support.[49,50,68,69,72,78] This could also be due to reduction of Ni in Ni–O–Ce by H_2, which was observed at temperatures above 400 °C.[77]

To examine the effect of the Ti dopant on the activity of Ni in DRM, temperature-dependent tests were conducted for 5 wt% Ni catalysts supported over all prepared $Ce_{1-x}Ti_xO_{2-\delta}$

supports. Prior to the studies, all samples were reduced at 750 °C in H_2 for 1 h. A total flow rate of 30 mL min^{-1} (N_2 : CH_4 : CO_2 = 10 : 10 : 10) was used for DRM. As shown in Fig. 3a and b, the percent conversion values of CO_2 and CH_4 reactants for all catalysts increase with increasing reaction temperature. The results are consistent with the endothermic nature of the DRM reaction.[3,6] A higher percent conversion value of CO_2 was observed compared to that of CH_4, which could be due to the reverse-water–gas shift (RWGS) reaction as a side reaction in DRM.[6,16] The ignition temperature and activity of catalysts vary with the composition of Ti dopant in $Ce_{1-x}Ti_xO_{2-\delta}$ supports. Ni over pure $CeO_{2-\delta}$ and $Ce_{0.9}Ti_{0.1}O_{2-\delta}$ exhibited a comparable DRM activity except during the temperature range between 550 and 750 °C. Compared to these two catalysts, $Ni/Ce_{0.8}Ti_{0.2}O_{2-\delta}$ showed a slightly lower activity in DRM, and further increase in the Ti composition resulted in a further decrease in the activity of $Ni/Ce_{1-x}Ti_xO_{2-\delta}$. As it is known that metallic Ni is the active species in DRM, the lower activity of Ni over ceria with high Ti amounts (*e.g.*, $Ce_{0.5}Ti_{0.5}O_{2-\delta}$) could be correlated with a significantly lower Ni metal dispersion value with a much lower metallic Ni amount present over the catalyst surface.[81,82]

5 wt% Ni catalysts over pure $CeO_{2-\delta}$ as well as over doped ceria with a low Ti composition ($Ce_{0.9}Ti_{0.1}O_{2-\delta}$) and a high Ti composition ($Ce_{0.5}Ti_{0.5}O_{2-\delta}$) were selected for stability tests at 750 °C for 24 h. The results shown in Fig. 3c and d were collected with a gas mixture of N_2, CH_4, and CO_2 with a flow rate of 10–10–10 mL min^{-1}, corresponding to a GHSV value of 18 000 mL g^{-1} h^{-1}. There is around 5% difference in the conversion values reported at 750 °C in the stability tests compared to those in temperature-dependent DRM results. This is likely due to the additional stepwise heating treatments in temperature-dependent DRM tests during which all catalysts were heated from 300 to 800 °C with a

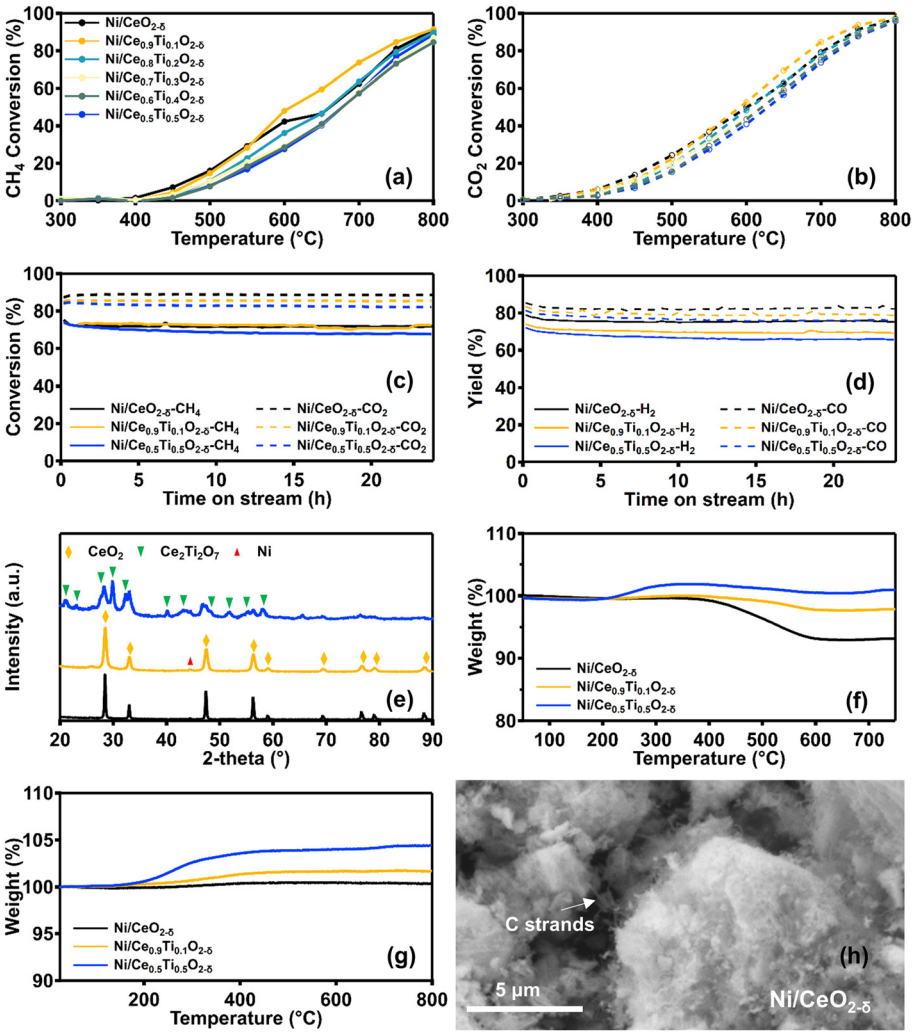

Fig. 3 (a) CH_4 and (b) CO_2 conversion values with respect to the reaction temperature between 300 and 800 °C collected from the DRM reaction over 5 wt% Ni supported on $Ce_{1-x}Ti_xO_{2-\delta}$ at a GHSV value of 18 000 mL g^{-1} h^{-1}; (c) CH_4 and CO_2 conversions and (d) H_2 and CO yields *versus* time on stream over 5 wt% Ni supported on $CeO_{2-\delta}$, $Ce_{0.9}Ti_{0.1}O_{2-\delta}$, and $Ce_{0.5}Ti_{0.5}O_{2-\delta}$ during the reaction at 750 °C at the same GHSV value; (e) XRD patterns of spent catalysts after stability tests; TGA results of (f) spent catalysts after stability tests and (g) reduced catalysts, respectively; (h) SEM results of spent $Ni/CeO_{2-\delta}$ after stability tests.

temperature increment of 50 °C under the reaction stream and held at each temperature for 0.5 h during the data collection. For the stability tests, all catalysts were directly heated up to 750 °C in a temperate ramp of 20 °C min^{-1} under the reaction stream. As shown in Fig. 3c and d, all three catalysts showed good stability with less than 5% loss of activity after 24 h. It is known that Ni-based catalysts are prone to deactivation due to carbon deposits in DRM.[15,83] Therefore, after the stability test, the TGA analysis (Fig. 3f) was carried out over spent catalysts for the investigation of carbon that was present over the catalyst surface, which was compared to that of reduced catalysts prepared prior to the DRM tests (Fig. 3g). In the temperature range between 400 and 600 °C, the weight loss in TGA data can be attributed to the oxidation of carbon to CO_2.[84] Our TGA results (Fig. 3f) in general suggest significantly less carbon deposits over Ni supported on Ti-doped ceria. The spent sample of $Ni/CeO_{2-\delta}$ showed around 7% weight loss due to carbon deposition. The carbon exhibits fiber-like features in the SEM image (Fig. 3h). However, only about 2 wt% or even a negligible amount of weight loss was detected in spent samples of $Ni/Ce_{0.9}Ti_{0.1}O_{2-\delta}$ and $Ni/Ce_{0.5}Ti_{0.5}O_{2-\delta}$. At around 350 °C, there is a weight increase of the catalysts, observed especially clearly for $Ni/Ce_{0.5}Ti_{0.5}O_{2-\delta}$ and this is attributed to the oxidation of the reduced catalyst as shown in Fig. 3g.[50] The same behavior was observed when we increased the GHSV value from 18 000 to 36 000 mL g^{-1} h^{-1} as shown in Fig. S4. The amount of carbon deposits over these samples followed the trend $Ni/Ce_{0.5}Ti_{0.5}O_{2-\delta} \ll Ni/Ce_{0.9}Ti_{0.1}O_{2-\delta} < Ni/CeO_{2-\delta}$. As suggested by combined catalyst characterization and activity studies, Ni catalysts supported over Ti-doped ceria exhibited an enhanced reducibility and a stronger metal–support interaction, which could promote the removal of carbon deposits in DRM.[85,86]

The XRD patterns of spent samples of Ni catalysts over $CeO_{2-\delta}$, $Ce_{0.9}Ti_{0.1}O_{2-\delta}$, and $Ce_{0.5}Ti_{0.5}O_{2-\delta}$ were obtained (Fig. 3e). Both samples of $Ni/CeO_{2-\delta}$ and $Ni/Ce_{0.9}Ti_{0.1}O_{2-\delta}$ maintained the fluorite structure of CeO_2. A small intensity at 44.5° was attributed to metallic Ni, confirming that Ni^0 is the active metal species during the DRM reaction. However, for the spent sample of $Ni/Ce_{0.5}Ti_{0.5}O_{2-\delta}$, the reflections due to CeO_2 became much boarder, indicating a less crystalline fluorite structure. The patterns related to TiO_2 were not clearly detected. Furthermore, new reflections at 21.3°, 23.2°, 27.8°, 30.1°, 32.3°, 40.3°, 43.3°, 48.4°, 52.0°, 55.2°, and 58.4° were observed which can be attributed to (210), (002), (400), (112), (410), (022), (420), (520), (114), (304) and (232) of $Ce_2Ti_2O_7$ (PDF #47-0667). This indicates a reduction of Ce^{4+} to Ce^{3+} and the formation of a new crystal phase of $Ce_2Ti_2O_7$ after sample reduction and the DRM reaction. Ruan and co-workers investigated the structure change between CeO_2–TiO_2 and $Ce_2Ti_2O_7$ and observed the transformation of CeO_2–TiO_2 mixed oxides into $Ce_2Ti_2O_7$, promoted by the dispersed Ni metal under reduction in CH_4.[48] Compared to pure ceria, $Ce_2Ti_2O_7$ has a higher oxygen mobility due to the disorder of both cations and anions in the sublattice.[87] Although $Ni/Ce_{0.5}Ti_{0.5}O_{2-\delta}$ delivered the least activity in DRM among all three catalysts, it showed very little carbon deposit. Such behavior could also be correlated with the enhanced oxygen mobility and redox properties due to the formation of $Ce_2Ti_2O_7$ in $Ni/Ce_{0.5}Ti_{0.5}O_{2-\delta}$.

Our study provides new insight into the role of Ti doping in the formation of Ni species over $Ce_{1-x}Ti_xO_{2-\delta}$ and associated activity and stability in DRM. The effect of the Ti^{4+} dopant over 5 wt% $Ni/Ce_{1-x}Ti_xO_{2-\delta}$ was previously studied by Damaskinos and co-workers.[33] They chose the Ti stoichiometry of x = 0.2 and 0.5. The fluorite structure of CeO_2 was maintained through the different concentrations of Ti^{4+} doping. After the doping of CeO_2 with Ti with the stoichiometry of 0.5, the diffraction peaks shifted to higher 2-theta angles in XRD, indicating a decrease in the lattice constant of ceria due to incorporation of Ti^{4+} ions in the CeO_2 lattice. Also, a broadening of peaks representing CeO_2 was observed for Ti-doped samples indicating a decrease in crystallite size of the support which correlated well with our XRD data. Although not mentioned in their study, the XRD pattern of 5 wt% $Ni/Ce_{0.5}Ti_{0.5}O_{2-\delta}$ seemed to suggest the formation of isolated titania domains and $NiTiO_3$, which are similar to what have been observed in our studies. For the DRM reactivity studies, they observed an increase in the CH_4 conversion and a significant decrease in carbon deposition for 5 wt% $Ni/Ce_{0.8}Ti_{0.2}O_{2-\delta}$ compared to the 5 wt% Ni/CeO_2 catalyst. However, the CH_4 conversion was lower for the 5 wt% $Ni/Ce_{0.5}Ti_{0.5}O_{2-\delta}$. This in general agrees well with our results which showed that a small amount of Ti dopant can enhance both the catalyst activity and the resistance to carbon in DRM due to the participation of lattice labile oxygen from the support for gasification of C, leading to the formation of CO.[33,35] With the control of the small increment of Ti dopant, our study demonstrated that 5 wt% $Ni/Ce_{0.9}Ti_{0.1}O_{2-\delta}$ gave the highest conversion of CH_4 compared to all the other catalysts, indicating that the small stoichiometry of 0.1 for Ti in $Ce_{1-x}Ti_xO_{2-\delta}$ delivers a good enhancement of the catalytic performance of Ni. A major difference observed between our study and the one performed by Damaskinos *et al.* was in the C resistance for $Ni/Ce_{0.5}Ti_{0.5}O_{2-\delta}$. Our results (Fig. 3f) clearly show that the spent 5 wt% $Ni/Ce_{0.5}Ti_{0.5}O_{2-\delta}$ catalyst had negligible C deposition compared to $Ni/CeO_{2-\delta}$ and $Ni/Ce_{0.9}Ti_{0.1}O_{2-\delta}$. As shown in Fig. 3e and Fig. S3, 5 wt% $Ni/Ce_{0.5}Ti_{0.5}O_{2-\delta}$ underwent a change in the crystal structure for CeO_2 during the reduction with H_2 at 750 °C and the DRM reaction, leading to the formation of $Ce_2Ti_2O_7$. It is known that $Ce_2Ti_2O_7$ has high O mobility that could facilitate the removal of deposited C.[60] Damaskinos and co-workers concluded higher C deposition over spent $Ni/Ce_{0.5}Ti_{0.5}O_{2-\delta}$ compared to 5 wt% $Ni/Ce_{0.8}Ti_{0.2}O_{2-\delta}$. They explained that this was due to the least participation of lattice labile O for removal of C in DRM as demonstrated in transient experiments using $^{18}O_2$ isotope species.[33] The exact nature for the difference between our results and the previous report is not clear, although there is a likelihood due to the differences in catalyst synthesis that could result in some variations in the size, structure, and composition of the

prepared samples. In particular, the Ti doping level plays an important role in the nature of synthesized ceria supports, which in turn could influence the formation of Ni species (NiO and $NiTiO_3$). Our group has confirmed the concentration of Ti for the prepared catalysts through ICP-OES studies with the stoichiometry of Ti matching the targeted values. The quantification of the amount of Ti dopant was not indicated in their study. Furthermore, it would be interesting to know if there was a composition and structure change for spent Ni/$Ce_{0.5}Ti_{0.5}O_{2-\delta}$.

To extrapolate the effect of Ti doping in ceria on the catalytic performance of other metals in DRM, our group carried out a study over Co catalysts considering that Co shows good DRM activity.[64,88] $Ce_{0.9}Ti_{0.1}O_{2-\delta}$-supported Co catalysts with both 5 and 10 wt% loadings were prepared considering that among the studied series of $Ce_{1-x}Ti_xO_{2-\delta}$, Ni supported over $Ce_{0.9}Ti_{0.1}O_{2-\delta}$ showed a good activity with a reasonable amount of carbon deposits during the DRM reaction. As a comparison, Co catalysts over pure ceria were also synthesized. As shown in Fig. 4a, the fluorite structure of ceria was observed in both ceria supports and all ceria-supported Co catalysts. No clear reflection peaks of Co species were observed for Co catalysts with a 5 wt% Co loading, and Co_3O_4 was identified with a peak located at 37.0° (PDF #42-1467) for the samples with a 10 wt% Co loading. This indicates that Co could maintain good dispersion as small particles over the support at a low weight loading (*i.e.*, 5 wt%). With higher amounts of Co (*i.e.*, 10 wt%), it can aggregate and form crystallite structures during calcination. Like the study of Ni as described above, a small decrease of 0.003 Å in the lattice constant of CeO_2 was detected with dispersed 5 wt% Co, which increased to 0.011 Å with dispersed 10 wt% Co. This is consistent with the suggestion of incorporation of Co into the ceria lattice.[89,90] The extent of formation of Co-doped ceria could be small when compared to the study by Yang and co-workers as they reported a reduction in the ceria lattice by ~0.019 Å for 2% atom doping of Co in ceria ($Ce_{0.98}Co_{0.02}O_{2-\delta}$)

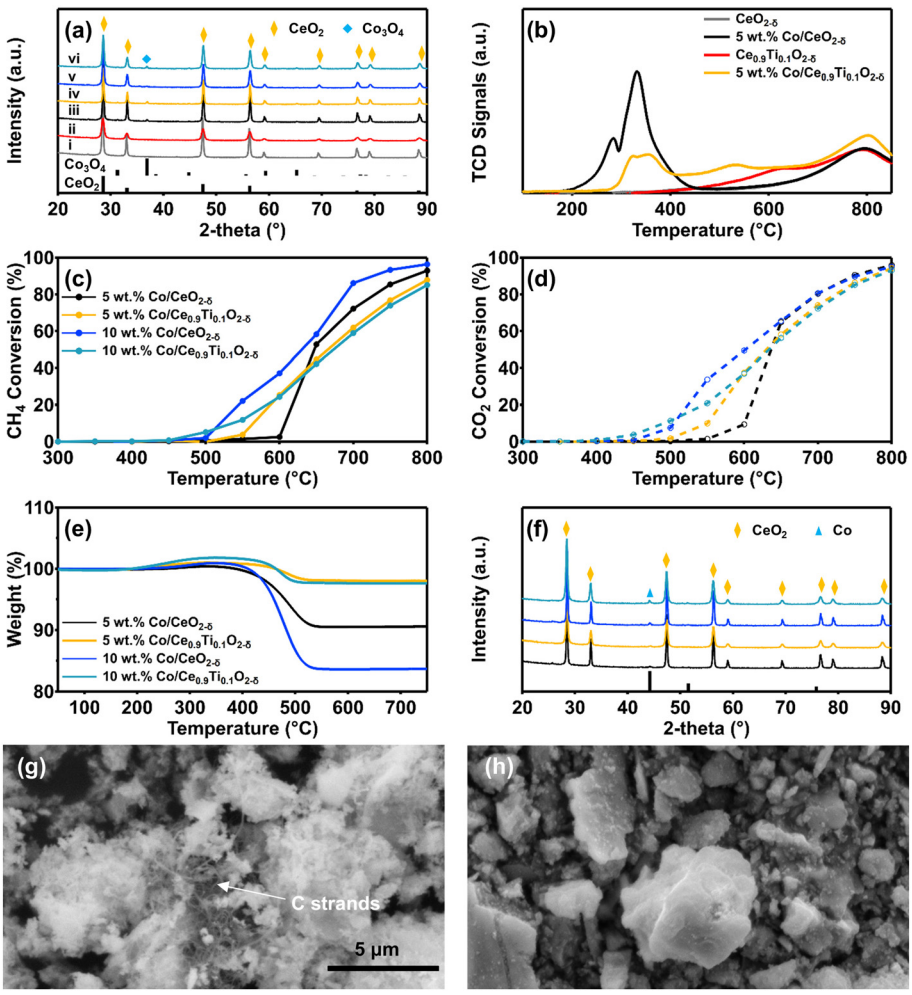

Fig. 4 (a) XRD patterns of (i) $CeO_{2-\delta}$, (ii) $Ce_{0.9}Ti_{0.1}O_{2-\delta}$, (iii) 5 wt% and (iv) 10 wt% Co over $CeO_{2-\delta}$, and (v) 5 wt% and (vi) 10 wt% Co over $Ce_{0.9}Ti_{0.1}O_{2-\delta}$; (b) TPR profiles of indicated Co catalysts and ceria supports; (c) CH_4 and (d) CO_2 conversion values with respect to the reaction temperature between 300 and 800 °C collected from the DRM reaction over 5 wt% and 10 wt% Co supported on $CeO_{2-\delta}$ and $Ce_{0.9}Ti_{0.1}O_{2-\delta}$ at a GHSV value of 18 000 mL g^{-1} h^{-1}; (e) TGA profiles and (f) XRD patterns of spent catalysts after DRM tests; SEM results of spent (g) 5 wt% Co/$CeO_{2-\delta}$ and (h) 5 wt% Co/$Ce_{0.9}Ti_{0.1}O_{2-\delta}$ catalysts after DRM tests.

and by 0.036 Å for 10% atom doping of Co in ceria ($Ce_{0.90}Co_{0.10}O_{2-\delta}$).[89] Fig. 4b shows the H_2-TPR profiles of both supports with and without 5 wt% Co. The reduction features between ~200 and 450 °C with two peaks at 284 and 332 °C from 5 wt% Co/$CeO_{2-\delta}$ were assigned to two reduction steps of Co_3O_4 to CoO and CoO to Co, respectively.[91–93] These two peaks representing stepwise reduction of Co_3O_4 are also present over 5 wt% Co/$Ce_{0.9}Ti_{0.1}O_{2-\delta}$. Additionally, a small reduction peak at 535 °C was observed in the TPR profile for 5 wt% Co/$Ce_{0.9}Ti_{0.1}O_{2-\delta}$, which could be due to the reduction of Co_3O_4 that has a strong interaction with Ti-doped ceria.[94] The temperature-dependent DRM results of Co over $CeO_{2-\delta}$ and $Ce_{0.9}Ti_{0.1}O_{2-\delta}$ are given in Fig. 4c and d. Prior to the DRM reaction, all catalysts were reduced at 750 °C under H_2 for 1 h, which reduced Co_3O_4 to metallic Co through a CoO transition as demonstrated in previous reports.[64,91,92,95,96] However, during the DRM reaction, it has been shown that the chemical state and/or structure of Co species along with the ceria support experience dynamic changes with respect to the temperature and gas species in the reaction stream.[64,97] In DRM, CoO can reappear at 200 °C and metallic Co becomes predominant with the increase of the reaction temperature to 500 °C, which are active species for methane activation. This is consistent with our XRD patterns of all spent samples of 5 and 10 wt% Co catalysts over $CeO_{2-\delta}$ and $Ce_{0.9}Ti_{0.1}O_{2-\delta}$ (Fig. 4f), which show metallic Co as evident with a small intensity at 44.2° (PDF #15-0806). For a 5 wt% Co loading, a clear decrease in the ignition temperature was observed for Co/$Ce_{0.9}Ti_{0.1}O_{2-\delta}$ compared to that of Co/$CeO_{2-\delta}$. With the increase of the Co loading to 10 wt%, the ignition temperatures for Co over both ceria supports were similar. For both 5 and 10 wt% Co loadings, Co over $Ce_{0.9}Ti_{0.1}O_{2-\delta}$ showed similar activity in DRM. However, the increase in the cobalt loading to 10 wt% increased the activity of Co/$CeO_{2-\delta}$ but at the cost of extensive formation of carbon deposits. TGA analysis indicated an increased weight loss from 5 to 16% due to carbon burn off as the weight loading of Co was increased from 5 to 10 wt% over the $CeO_{2-\delta}$ support (Fig. 4e). On the other hand, both $Ce_{0.9}Ti_{0.1}O_{2-\delta}$-supported Co catalysts showed a weight loss of around 2%. As shown in the SEM images (Fig. 4g and h), there is little evidence of carbon deposition over the spent sample of 5 wt% Co/$Ce_{0.9}Ti_{0.1}O_{2-\delta}$. However, filamentous carbon-like features were clearly observed over 5 wt% Co/$CeO_{2-\delta}$. Similar to Ni, Ti doping in ceria has a promotional effect on the redox properties of ceria and the interaction of supported Co catalysts that help remove carbon deposits during the DRM reaction.

Conclusions

In summary, $Ce_{1-x}Ti_xO_{2-\delta}$ supports were synthesized using a sol–gel method with controlled Ti compositions (x = 0–0.5). At a low composition of Ti dopant ($x < 0.3$), Ti can be more well incorporated into the ceria lattice to form $Ce_{1-x}Ti_xO_{2-\delta}$ mixed oxides while maintaining the fluorite structure of ceria. Further introducing Ti into ceria produces additional TiO_2 crystallites. Ti doping enhances the reducibility of ceria as additional reduction features were observed related to Ce^{4+} in Ce–O–Ti structures at lower temperatures compared to that of Ce^{4+} in bulk ceria. 5 wt% Ni was prepared over $Ce_{1-x}Ti_xO_{2-\delta}$ and the composition of Ti dopant in $Ce_{1-x}Ti_xO_{2-\delta}$ plays a role in the formation of Ni species. NiO is the major species over doped-ceria with a very low amount of Ti dopant (*e.g.*, $Ce_{0.9}Ti_{0.1}O_{2-\delta}$), while $NiTiO_3$ becomes the predominant component over $Ce_{1-x}Ti_xO_{2-\delta}$ with high Ti composition values (*i.e.*, $Ce_{0.5}Ti_{0.5}O_{2-\delta}$). Compared to Ni/$CeO_{2-\delta}$, Ni/$Ce_{0.9}Ti_{0.1}O_{2-\delta}$ delivers better activity in DRM, which can be attributed to the enhanced reducibility of Ti-doped ceria and the stronger metal–support interaction by a small amount of Ti doping. The lower activity was observed over Ni/$Ce_{0.5}Ti_{0.5}O_{2-\delta}$ in DRM, which can be due to the formation of $NiTiO_3$ that produces significantly less metallic Ni as the active species for DRM compared to NiO formed over $CeO_{2-\delta}$ and $Ce_{0.9}Ti_{0.1}O_{2-\delta}$. Characterization of spent samples showed a significant enhancement in carbon resistance in Ni catalysts supported over Ti-doped ceria. After a 24 h reaction on stream, a significant amount of weight loss was detected for Ni/$CeO_{2-\delta}$ due to the carbon removal. Less carbon was found over the spent Ni/$Ce_{0.9}Ti_{0.1}O_{2-\delta}$ sample and the Ni/$Ce_{0.5}Ti_{0.5}O_{2-\delta}$ catalyst even showed no clear sign of carbon deposition. The formation of a new $Ce_2Ti_2O_7$ phase in spent Ni/$Ce_{0.5}Ti_{0.5}O_{2-\delta}$ could better help remove carbon deposits. Our results clearly demonstrate that the Ti dopant can modify the crystal structures, surface properties, and redox properties of ceria, which can affect the formation of supported Ni species and thus influence their activity, stability, and carbon resistance in the DRM reaction. Similar effects of the Ti dopant were also found in ceria-supported Co catalysts.

Author contributions

Jintao Miao: sample preparation, experiments, data collection and analysis of Ni catalysts over $Ce_{1-x}Ti_xO_{2-\delta}$, original manuscript writing and following editing. Nishan Paudyal: sample preparation, experiments, data collection and analysis of Co catalysts over $CeO_{2-\delta}$ and $Ce_{0.9}Ti_{0.1}O_{2-\delta}$, original manuscript writing and following editing. Rosa V. Melinda: sample preparation and XRD experiment of TiO_2. Jing Zhou: funding acquisition, supervision, and manuscript review and revision.

Conflicts of interest

The authors declare no competing financial interest.

Data availability

Supplementary information: additional figures, tables, and further experimental details as well as data analysis as indicated in the article are provided. See DOI: **https://doi.org/10.1039/D5CY00760G**.

The authors confirm that the data supporting the findings of this study are available within the article and its SI.

Acknowledgements

This research work is financially supported by the Wyoming Carbon Engineering Initiative from the School of Energy Resources and SI Seed Grant (BFD-SISGHOBERG) for Center for Energy Materials at the University of Wyoming (UW) as well as by the U.S. National Science Foundation under Grant CHE-2154622. We thank Dr. Wenqian Xu from Argonne National Laboratory for his help with the synchrotron XRD experiments, Xerxes Steirer from Colorado School of Mines for his help with XPS experiments, Janet Dewey from the Geochemistry Analytical Laboratory at UW for the assistance with the ICP-OES tests, and Dr. Tyler C. Brown from the Materials Characterization Laboratory at UW for the help with the SEM experiments.

References

1 H. O. Seo, *Catalysts*, 2018, **8**, 18.
2 M. Mohamedali, A. Henni and H. Ibrahim, *ChemEngineering*, 2018, **2**, 9.
3 S. Bhattar, M. A. Abedin, S. Kanitkar and J. J. Spivey, *Catal. Today*, 2021, **365**, 2–23.
4 M. Yusuf, A. S. Farooqi, L. K. Keong, K. Hellgardt and B. Abdullah, *Chem. Eng. Sci.*, 2021, **229**, 116072.
5 S. B. Wang, G. Q. M. Lu and G. J. Millar, *Energy Fuels*, 1996, **10**, 896–904.
6 D. Pakhare and J. Spivey, *Chem. Soc. Rev.*, 2014, **43**, 7813–7837.
7 W. N. Manan, W. Isahak and Z. Yaakob, *Catalysts*, 2022, **12**, 452.
8 T. Montini, M. Melchionna, M. Monai and P. Fornasiero, *Chem. Rev.*, 2016, **116**, 5987–6041.
9 A. G. S. Hussien and K. Polychronopoulou, *Nanomaterials*, 2022, **12**, 3400.
10 N. A. Harry, S. Saranya, S. M. Ujwaldev and G. Anilkumar, *Catal. Sci. Technol.*, 2019, **9**, 1726–1743.
11 Z. Y. Liu, D. C. Grinter, P. G. Lustemberg, T. D. Nguyen-Phan, Y. H. Zhou, S. Luo, I. Waluyo, E. J. Crumlin, D. J. Stacchiola, J. Zhou, J. Carrasco, H. F. Busnengo, M. V. Ganduglia-Pirovano, S. D. Senanayake and J. A. Rodriguez, *Angew. Chem., Int. Ed.*, 2016, **55**, 7455–7459.
12 Z. Y. Liu, P. Lustemberg, R. A. Gutierrez, J. J. Carey, R. M. Palomino, M. Vorokhta, D. C. Grinter, P. J. Ramirez, V. Matolin, M. Nolan, M. V. Ganduglia-Pirovano, S. D. Senanayake and J. A. Rodriguez, *Angew. Chem., Int. Ed.*, 2017, **56**, 13041–13046.
13 L. Baharudin, N. Rahmat, N. H. Othman, N. Shah and S. S. A. Syed-Hassan, *J. CO2 Util.*, 2022, **61**, 102050.
14 C. Vogt, J. Kranenborg, M. Monai and B. M. Weckhuysen, *ACS Catal.*, 2020, **10**, 1428–1438.
15 M. D. Argyle and C. H. Bartholomew, *Catalysts*, 2015, **5**, 145–269.
16 E. le Sache and T. R. Reina, *Prog. Energy Combust. Sci.*, 2022, **89**, 100970.
17 K. Chang, H. C. Zhang, M. J. Cheng and Q. Lu, *ACS Catal.*, 2020, **10**, 613–631.
18 N. V. Skorodumova, S. I. Simak, B. I. Lundqvist, I. A. Abrikosov and B. Johansson, *Phys. Rev. Lett.*, 2002, **89**, 166601.
19 A. Salcedo, P. G. Lustemberg, N. Rui, R. M. Palomino, Z. Liu, S. Nemsak, S. D. Senanayake, J. A. Rodriguez, M. V. Ganduglia-Pirovano and B. Irigoyen, *ACS Catal.*, 2021, **11**, 8327–8337.
20 J. A. Rodriguez, D. C. Grinter, Z. Liu, R. M. Palomino and S. D. Senanayake, *Chem. Soc. Rev.*, 2017, **46**, 1824–1841.
21 N. Paudyal, L. D. Hill, E. W. Peterson, N. J. Rifat, Y. Xu and J. Zhou, *J. Phys. Chem. C*, 2025, **129**, 10676–10684.
22 P. Min, S. Z. Zhang, Y. H. Xu and R. X. Li, *Appl. Surf. Sci.*, 2018, **448**, 435–443.
23 I. Luisetto, S. Tuti, C. Romano, M. Boaro and E. Di Bartolomeo, *J. CO2 Util.*, 2019, **30**, 63–78.
24 A. Kambolis, H. Matralis, A. Trovarelli and C. Papadopoulou, *Appl. Catal., A*, 2010, **377**, 16–26.
25 S. M. Lima, J. M. Assaf, M. A. Pena and J. L. G. Fierro, *Appl. Catal., A*, 2006, **311**, 94–104.
26 S. S. Kim, S. M. Lee, J. M. Won, H. J. Yang and S. C. Hong, *Chem. Eng. J.*, 2015, **280**, 433–440.
27 F. Zhang, Z. Y. Liu, X. B. Chen, N. Rui, L. E. Betancourt, L. L. Lin, W. Q. Xu, C. J. Sun, A. M. M. Abeykoon, J. A. Rodriguez, J. Terzan, K. Lorber, P. Djinovic and S. D. Senanayake, *ACS Catal.*, 2020, **10**, 3274–3284.
28 G. I. Siakavelas, N. D. Charisiou, S. AlKhoori, A. A. AlKhoori, V. Sebastian, S. J. Hinder, M. A. Baker, I. V. Yentekakis, K. Polychronopoulou and M. A. Goula, *Appl. Catal., B*, 2021, **282**, 119562.
29 M. Nakayama and M. Martin, *Phys. Chem. Chem. Phys.*, 2009, **11**, 3241–3249.
30 S. Watanabe, X. Ma and C. Song, *J. Phys. Chem. C*, 2009, **113**, 14249–14257.
31 Y. Zhou and J. Zhou, *J. Phys. Chem. Lett.*, 2010, **1**, 1714–1720.
32 M. Nolan, *J. Phys. Chem. C*, 2009, **113**, 2425–2432.
33 C. M. Damaskinos, M. A. Vasiliades and A. M. Efstathiou, *Appl. Catal., A*, 2019, **579**, 116–129.
34 K. C. Petallidou, K. Polychronopoulou, S. Boghosian, S. Garcia-Rodriguez and A. M. Efstathiou, *J. Phys. Chem. C*, 2013, **117**, 25467–25477.
35 C. M. Damaskinos, J. Zavašnik, P. Djinović and A. M. Efstathiou, *Appl. Catal., B*, 2021, **296**, 120321.
36 J. W. Han, J. S. Park, M. S. Choi and H. Lee, *Appl. Catal., B*, 2017, **203**, 625–632.
37 R. O. da Fonseca, A. R. Ponseggi, R. C. Rabelo-Neto, R. C. C. Simões, L. V. Mattos and F. B. Noronha, *J. CO2 Util.*, 2022, **57**, 101880.
38 B. H. Toby and R. B. Von Dreele, *J. Appl. Crystallogr.*, 2013, **46**, 544–549.
39 M. N. Abu Tahari, F. Salleh, T. S. Tengku Saharuddin, A. Samsuri, S. Samidin and M. A. Yarmo, *Int. J. Hydrogen Energy*, 2021, **46**, 24791–24805.
40 T. Matsuda, A. Hanai, F. Uchijima, H. Sakagami and N. Takahashi, *Bull. Chem. Soc. Jpn.*, 2002, **75**, 1165–1171.
41 W. Deng, Q. Dai, Y. Lao, B. Shi and X. Wang, *Appl. Catal., B*, 2016, **181**, 848–861.

42 R. D. Shannon, *Acta Crystallogr., Sect. A:Found. Crystallogr.*, 1976, **32**, 751–767.
43 D. J. Kim, *J. Am. Ceram. Soc.*, 1989, **72**, 1415–1421.
44 M. Nolan, *J. Phys. Chem. C*, 2011, **115**, 6671–6681.
45 Z. S. Lu, Z. X. Yang, B. L. He, C. Castleton and K. Hermansson, *Chem. Phys. Lett.*, 2011, **510**, 60–66.
46 K. Luo, M. R. Roberts, R. Hao, N. Guerrini, D. M. Pickup, Y.-S. Liu, K. Edström, J. Guo, A. V. Chadwick, L. C. Duda and P. G. Bruce, *Nat. Chem.*, 2016, **8**, 684–691.
47 F. P. Lu, B. B. Jiang, J. D. Wang, Z. L. Huang, Z. W. Liao, Y. R. Yang and J. Zheng, *RSC Adv.*, 2017, **7**, 22017–22026.
48 C. Ruan, Z.-Q. Huang, J. Lin, L. Li, X. Liu, M. Tian, C. Huang, C.-R. Chang, J. Li and X. Wang, *Energy Environ. Sci.*, 2019, **12**, 767–779.
49 J. L. Ye, Y. Q. Wang, Y. Liu and H. Wang, *Int. J. Hydrogen Energy*, 2008, **33**, 6602–6611.
50 Y. Zhang, Z. Li, X. Wen and Y. Liu, *Chem. Eng. J.*, 2006, **121**, 115–123.
51 Y. Mordekovitz, L. Shelly and S. Hayun, *J. Am. Ceram. Soc.*, 2019, **102**, 6957–6967.
52 M. Luo, J. Chen, L. Chen, J. Lu, Z. Feng and C. Li, *Chem. Mater.*, 2001, **13**, 197–202.
53 G. R. Rao, *Bull. Mater. Sci.*, 1999, **22**, 89–94.
54 J. Ding, Q. Zhong and S. Zhang, *Ind. Eng. Chem. Res.*, 2015, **54**, 2012–2022.
55 D. Jiang, S. L. Zhang, Y. Q. Zeng, P. F. Wang and Q. Zhong, *Catalysts*, 2018, **8**, 14.
56 G. S. Otero, P. G. Lustemberg, F. Prado and M. V. Ganduglia-Pirovano, *J. Phys. Chem. C*, 2020, **124**, 625–638.
57 Z. Hu and H. Metiu, *J. Phys. Chem. C*, 2011, **115**, 17898–17909.
58 G. Dutta, U. V. Waghmare, T. Baidya, M. S. Hegde, K. R. Priolkar and P. R. Sarode, *Chem. Mater.*, 2006, **18**, 3249–3256.
59 E. Smal, Y. Bespalko, M. Arapova, V. Fedorova, K. Valeev, N. Eremeev, E. Sadovskaya, T. Krieger, T. Glazneva, V. Sadykov and M. Simonov, *Int. J. Mol. Sci.*, 2023, **24**, 9680.
60 A. P. Anantharaman and H. P. Dasari, *Ceram. Int.*, 2021, **47**, 4367–4388.
61 S. Sameshima, M. Kawaminami and Y. Hirata, *J. Ceram. Soc. Jpn.*, 2002, **110**, 597–600.
62 J. Zhang, C. Ke, H. Wu, J. Yu and J. Wang, *J. Solid State Chem.*, 2016, **243**, 57–61.
63 Y. Kuru, S. R. Bishop, J. J. Kim, B. Yildiz and H. L. Tuller, *Solid State Ionics*, 2011, **193**, 1–4.
64 F. Zhang, Z. Y. Liu, S. H. Zhang, N. Akter, R. M. Palomino, D. Voychok, I. Orozco, D. Salazar, J. A. Rodriguez, J. Llorca, J. Lee, D. Kim, W. Q. Xu, A. I. Frenkel, Y. Y. Li, T. Kim and S. D. Senanayake, *ACS Catal.*, 2018, **8**, 3550–3560.
65 J. E. Sutton, A. Beste and S. H. Overbury, *Phys. Rev. B: Condens. Matter Mater. Phys.*, 2015, **92**, 144105.
66 I. Ganesh, A. K. Gupta, P. P. Kumar, P. S. C. Sekhar, K. Radha, G. Padmanabham and G. Sundararajan, *Sci. World J.*, 2012, **2012**, 1–16.
67 F. Dönmez and N. Ayas, *Int. J. Hydrogen Energy*, 2021, **46**, 29314–29322.
68 D. Hu, C. Liu, L. Li, K. L. Lv, Y. H. Zhang and J. L. Li, *Int. J. Hydrogen Energy*, 2018, **43**, 21345–21354.
69 Q. G. Yan, W. Z. Weng, H. L. Wan, H. Toghiani, R. K. Toghiani and C. U. Pittman, *Appl. Catal., A*, 2003, **239**, 43–58.
70 L. Li, B. Jiang, D. Tang, Z. Zheng and C. Zhao, *Catalysts*, 2018, **8**, 257.
71 W. X. Zou, C. Y. Ge, M. Y. Lu, S. G. Wu, Y. Z. Wang, J. F. Sun, Y. Pu, C. J. Tang, F. Gao and L. Dong, *RSC Adv.*, 2015, **5**, 98335–98343.
72 J. M. Jehng and C. M. Chen, *Catal. Lett.*, 2001, **77**, 147–154.
73 I. Iglesias, A. Quindimil, F. Marino, U. De-La-Torre and J. R. Gonzalez-Velasco, *Int. J. Hydrogen Energy*, 2019, **44**, 1710–1719.
74 A. Wolfbeisser, O. Sophiphun, J. Bernardi, J. Wittayakun, K. Fottinger and G. Rupprechter, *Catal. Today*, 2016, **277**, 234–245.
75 R. A. Demmin, C. S. Ko and R. J. Gorte, *J. Phys. Chem.*, 1985, **89**, 1151–1154.
76 S. Mahammadunnisa, P. M. K. Reddy, N. Lingaiah and C. Subrahmanyam, *Catal. Sci. Technol.*, 2013, **3**, 730–736.
77 G. Zhou, L. Barrio, S. Agnoli, S. D. Senanayake, J. Evans, A. Kubacka, M. Estrella, J. C. Hanson, A. Martínez-Arias, M. Fernández-García and J. A. Rodriguez, *Angew. Chem., Int. Ed.*, 2010, **49**, 9680–9684.
78 A. Romero-Núñez and G. Díaz, *RSC Adv.*, 2015, **5**, 54571–54579.
79 S. H. Zhang, J. Lee, D. H. Kim and T. Kim, *Catal. Sci. Technol.*, 2020, **10**, 2359–2368.
80 S. M. Sun, X. L. Zhao, H. Lu, Z. D. Zhang, J. J. Wei and Y. Z. Yang, *CrystEngComm*, 2013, **15**, 1370–1376.
81 B. Bachiller-Baeza, C. Mateos-Pedrero, M. A. Soria, A. Guerrero-Ruiz, U. Rodemerck and I. Rodriguez-Ramos, *Appl. Catal., B*, 2013, **129**, 450–459.
82 M. Radlik, M. Adamowska-Teyssier, A. Krzton, K. Koziel, W. Krajewski, W. Turek and P. Da Costa, *C. R. Chim.*, 2015, **18**, 1242–1249.
83 S. Wang and G. Q. Lu, in *Reaction Engineering for Pollution Prevention*, ed. M. A. Abraham and R. P. Hesketh, Elsevier Science, Amsterdam, 2000, ch. 8, pp. 75–84, DOI: **10.1016/B978-044450215-5/50080-9**.
84 A. E. Awadallah, A. A. Aboul-Enein and A. K. Aboul-Gheit, *Fuel*, 2014, **129**, 27–36.
85 H. A. Lara-Garcia, D. G. Araiza, M. Mendez-Galvan, S. Tehuacanero-Cuapa, A. Gomez-Cortes and G. Diaz, *RSC Adv.*, 2020, **10**, 33059–33070.
86 E. le Sache, J. L. Santos, T. J. Smith, M. A. Centeno, H. Arellano-Garcia, J. A. Odriozola and T. R. Reina, *J. CO2 Util.*, 2018, **25**, 68–78.
87 J. Xu, R. Xi, X. Xu, Y. Zhang, X. Feng, X. Fang and X. Wang, *J. Rare Earths*, 2020, **38**, 840–849.
88 Y. H. Sun, Y. B. Zhang, X. F. Yin, C. H. Zhang, Y. Li and J. Bai, *Green Chem.*, 2024, **26**, 5103–5126.
89 S. Sun, X. Zhao, H. Lu, Z. Zhang, J. Wei and Y. Yang, *CrystEngComm*, 2013, **15**, 1370.

90 Y.-N. Ou, G.-R. Li, J.-H. Liang, Z.-P. Feng and Y.-X. Tong, *J. Phys. Chem. C*, 2010, **114**, 13509–13514.
91 A. Parastaev, V. Muravev, E. Huertas Osta, A. J. F. van Hoof, T. F. Kimpel, N. Kosinov and E. J. M. Hensen, *Nat. Catal.*, 2020, **3**, 526–533.
92 S. S. Y. Lin, H. Daimon and S. Y. Ha, *Appl. Catal., A*, 2009, **366**, 252–261.
93 F. L. S. Carvalho, Y. J. O. Asencios, J. D. A. Bellido and E. M. Assaf, *Fuel Process. Technol.*, 2016, **142**, 182–191.
94 J. Mei, S. Zhao, H. Xu, Z. Qu and N. Yan, *RSC Adv.*, 2016, **6**, 31181–31190.
95 T. Paryjczak, J. Rynkowski and S. Karski, *J. Chromatogr.*, 1980, **188**, 254–256.
96 L. J. Garces, B. Hincapie, R. Zerger and S. L. Suib, *J. Phys. Chem. C*, 2015, **119**, 5484–5490.
97 K. X. Deng, Y. X. Wang, P. Pérez-Bailac, W. Q. Xu, J. Llorca, A. Martinez-Arias, D. N. Zakharov and J. A. Rodriguez, *J. Am. Chem. Soc.*, 2025, **147**, 19239–19252.

